Hochschule für Angewandte Wissenschaften Hamburg
Hamburg University of Applied Sciences

HAW Hamburg
Fakultät Technik und Informatik
Department Maschinenbau und Produktion

Introduction to Modal Analysis

Stefan Walter

27. November 2011

Acknowledgement

This introductory tutorial to modal analysis basically comprises two chapters of the author's Master Thesis with the title 'Investigation of different excitation and analysis methods for the modal testing of large airplane structures by means of a virtual test environment'. This thesis has been written in collaboration with Airbus Operations GmbH as part of a research project with the goal to identify the dynamic characteristics of an aircraft fuselage structure. The author would like to thank Airbus Operations for the opportunity to be a part of this highly interesting project and for providing him with the equipment necessary to succesfully complete his work. Furthermore, the author would like to thank his supervisors Christian Busch and Prof. Frank Ihlenburg for their continuous support and valuable advice during the course of this work.

List of Symbols and Abbreviations

Latin symbols

$A(j\omega)$	Accelerance FRF	$mm/(N\,s^2)$
$\left[C\right]$	Damping matrix	$(N\,s)/mm$
$\left\{f(t)\right\}$	External load vector	N
f	Frequency	Hz
j	Imaginary unit	$-$
$\left[K\right]$	Stiffness matrix	N/mm
$\left[M\right]$	Mass matrix	t
$p(t)$	Excitation signal	$var.$
$P(j\omega)$, $P(f)$	DFT of excitation signal	$var.$
p_0	(Maximum) amplitude of excitation signal	$var.$
t	Time	s
T	Periodic time	s
w_{eff}	Effective pulsewidth	s
$\left\{x(t)\right\}$	Deflection	mm
$\left\{\dot{x}(t)\right\}$	Velocity	mm/s
$\left\{\ddot{x}(t)\right\}$	Acceleration	mm/s^2
$Y(j\omega)$	Mobility FRF	$mm/(N\,s)$

Greek symbols

$\alpha(j\omega)$	Receptance FRF	mm/N

ζ		Damping factor (relative to critical damping)	$-$
Θ		Angle	rad
σ		Dilation/ compression factor	s^2
	or :	Standard deviation	$var.$
τ		Time shift	s
$\left[\Phi\right]$		Matrix of eigenvectors	$-$
Ω, ω		Angular frequency	rad/s

Indices and superscripts

$\left[\cdots\right]^{-1}$		Inverse matrix
$(\cdots)_i$		Related to i^{th} eigenmode
	or :	i^{th} component of vector
$(\cdots)_{ij}$		Matrix element in i^{th} row and j^{th} column
$(\cdots)_r$, $(\cdots)_0$		Resonance (angular) frequency

Abbreviations

CFT	Continuous Fourier Transform
DFT	Discrete Fourier Transform
DoF	Degree(s) of freedom
FE	Finite Element
FFT	Fast Fourier Transform
FRF	Frequency Response Function
FT	Fourier Transform
LSCE	Least-squares Complex Exponential
MDoF	Multi-degree-of-freedom
RD	Random Decrement
SDoF	Single-degree-of-freedom
STFT	Short-time Fourier Transform

1 Excitation methods

There is a wide range of possible excitation signals for modal testing, each of them with their specific advantages and drawbacks. Fig. 1.1 gives a general overview of the available signal types. The signal types to be investigated in the present work are accentuated.

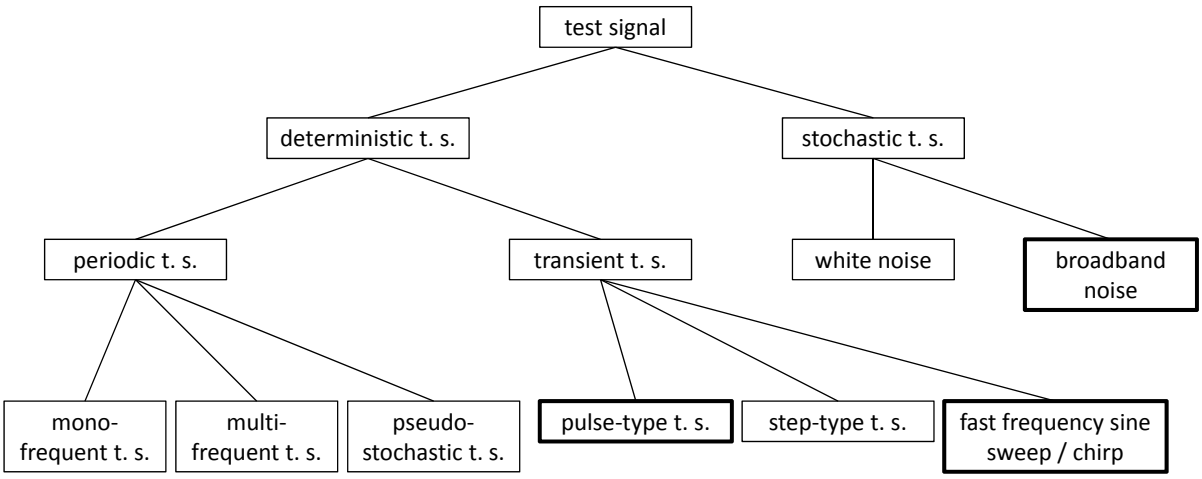

Abbildung 1.1: Classification of excitation signals [10, translated from German]

The following sections shall describe the signals which are to be investigated in the present work in detail, beginning with the most commonly used excitation type for modal testing, the sine sweep.

1.1 Sine sweep excitation

The most commonly used excitation method for modal testing is the sine sweep or chirp. There are three different types of sine sweeps which differ in the rate of change of the angular frequency: linear, exponential and logarithmical sine sweep. Each of them shall be mathematically defined in the following subsections with the mathematical definitions taken from [10]. Furthermore, a graphical depiction of the signals in time and frequency domain shall be given and the characteristic properties of each signal type shall be discussed.

1.1.1 Linear sine sweep

The angular frequency of the linear sine sweep, Ω, is a linear function of time instead of being a constant as with the classical harmonic excitation signal. The linear sweep is defiend by the following formula:

$$p(t) = p_0 \sin\Theta = p_0 \sin((a + b\,t)\,t) \tag{1.1}$$

with the momentary angular frequency

$$\Omega = \frac{d\Theta}{dt} = a + 2\,b\,t \tag{1.2a}$$

and the constants

$$a = \Omega_a \ , \ b = \frac{\Omega_b - \Omega_a}{2\,T} \tag{1.2b}$$

A typical linear sine sweep signal is shown in fig. 1.2, in both frequency and time domain. As the rate of change of Ω is constant in time, the frequency spectrum of the linear sine sweep remains nearly constant throughout the covered frequency range.

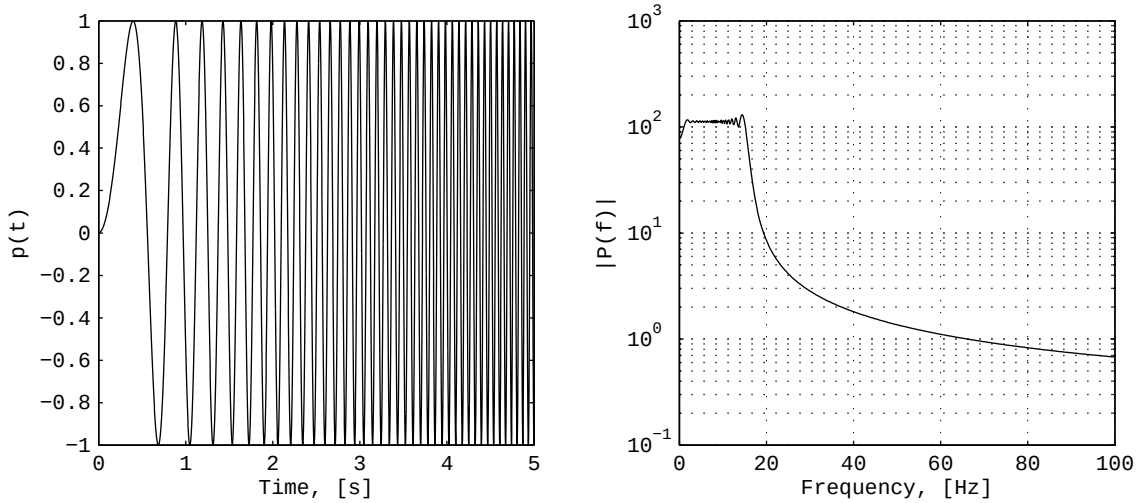

Abbildung 1.2: Linear sine sweep (time and frequency domain)

1.1.2 Exponential sine sweep

The mathematical definition of an exponential sine sweep signal is given by eq. 1.3:

$$p(t) = p_0 \sin\Theta = p_0 \sin\left(\frac{\Omega_a}{a}\,\exp\left(a\,t\right)\right) \tag{1.3}$$

with the momentary angular frequency

$$\Omega = \frac{d\Theta}{dt} = \Omega_a \, \exp\left(a\, t\right) \tag{1.4}$$

The angular frequency of the exponential sine sweep follows an exponential law, i.e. the rate of change of Ω increases with time. Therefore, as higher frequencies are passed faster the spectrum shows a decreasing characteristic, as evidenced by fig. 1.3.

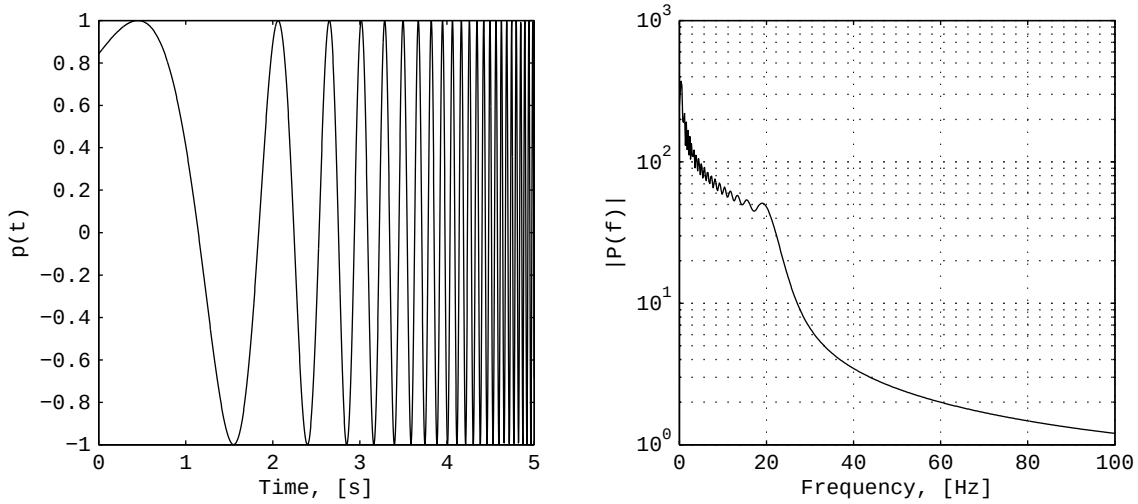

Abbildung 1.3: Exponential sine sweep (time and frequency domain)

1.1.3 Logarithmical sine sweep

Finally, the logarithmical sine sweep is defined by:

$$p(t) = p_0 \, \sin\Theta = p_0 \, \sin\left(-\frac{1}{b} \, \ln(a - b\, t)\right) \tag{1.5}$$

with the momentary angular frequency

$$\Omega = \frac{d\Theta}{dt} = \frac{1}{a - b\, t} \tag{1.6}$$

For the logarithmical sine sweep, Θ changes logarithmically with time which means that, as with the exponential sweep, the rate of change of Ω grows faster with time. The spectrum of a logarithmical sweep signal correspondingly shows a qualitatively similar characteristic to that of the exponential sweep.

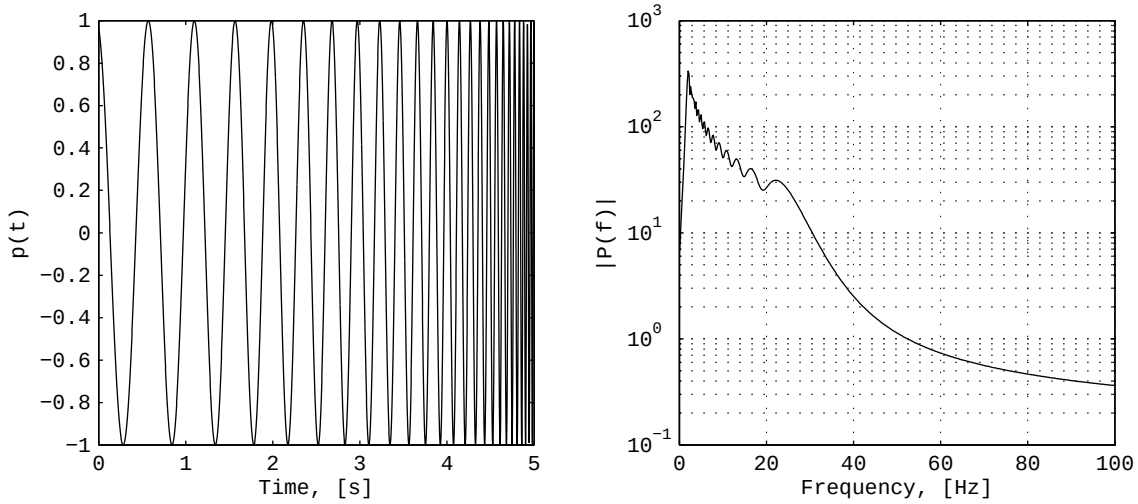

Abbildung 1.4: Logarithmical sine sweep (time and frequency domain)

1.2 Impulse excitation

An alternative approach to sine sweep excitation is presented by structural excitation using impulse signals. Impulse signals are compactly supported in time, i.e. they rapidly decay to zero. This characteristic allows the application of time domain modal analysis techniques which are based on the free decay of a structural response. Furthermore, a reduction of expensive testing time might be accomplished using short pulses rather than slow sweeps as excitation signals. For that reason different types of impulse signals originally designed for a signal analysis technique called Wavelet analysis have been modified to suit the specific requirements of an excitation signal and investigated with respect to their suitability for modal testing. Those signals, namely the Morlet, Mexican Hat and Shannon wavelets, as well as the modifications applied to them shall be described in the following sections, beginning with the a description of the modifications that had to be applied.

1.2.1 Usage of wavelets for structural excitation

As previously mentioned, the wavelet pulses were originally developed in the context of Wavelet analysis, a signal processing technique used to analyse not only the frequency content of signals but also the time at which certain components are present. Wavelet analysis can be seen as an enhancement of the Short-time Fourier Transform (STFT) because certain drawbacks of the STFT are reduced in Wavelet analysis. In addition to that, Wavelet analysis is also used for data compression. Taking into account the purpose for which wavelets were originally designed, it becomes obvious that certain modifications are necessary to make them applicable for structural excitation. First of all, many wavelets are formulated in complex space. As the imaginary part of a complex number does not have any meaning regarding the mechanical excitation of a structure, the complex exponentials have to be changed to cosine functions, i.e. only the real

part of the orignal functions is to be adopted. Furthermore, Wavelet analysis requires a certain interdependence between the parameters frequency (also called scale in Wavelet analysis theory), amplitude and extension in time (or support) of the wavelet. Those requirements are due to considerations like energy conservation and the uncertainty principle which are not relevant for the application of the impulses as structural excitation signals. Therefore, this interdependency has been given up and the parameters p_0 and σ have been introduced to independently specify the amplitude and width of the pulses. Finally, the parameter τ has been introduced to shift the pulses in time. Thus, it becomes possible to define a series of pulses which are successively applied to the structure to investigate several effects in one single simulation respectively test run.

1.2.2 Morlet wavelet impulse

The initial formula of the Morlet wavelet has been taken from [9]:

$$p(t) = \pi^{-\frac{1}{4}} \exp\left(-\frac{t^2}{2}\right) \exp(j\,\Omega\,t) \tag{1.7}$$

After application of the adaptions described in the previous section, the modified equation of the Morlet wavelet impulse is as follows:

$$p(t) = p_0 \exp\left(-\frac{(t-\tau)^2}{2\,\sigma}\right) \cos(\Omega\,(t-\tau)) \tag{1.8}$$

with

$$\sigma = -\frac{w_{eff}^2}{8 \ln 0.001} \tag{1.9a}$$

w_{eff} = effective width of the pulse, as defined by

$$p\left(\tau \pm \frac{w_{eff}}{2}\right) = 0.001\,p_0 \tag{1.9b}$$

The effective width of the pulse has been introduced so the user can more conveniently specify the width of the pulse than this would have been possible by directly setting the value of the quantity σ. The factor 0.001, which means that the pulse is considered to be over once the amplitude has decayed to one thousandth of the maximum amplitude, has been chosen arbitrarily after trying out several values and inspecting the results optically.

Fig. 1.5 shows the thus defined Morlet wavelet in both time and frequency domain.

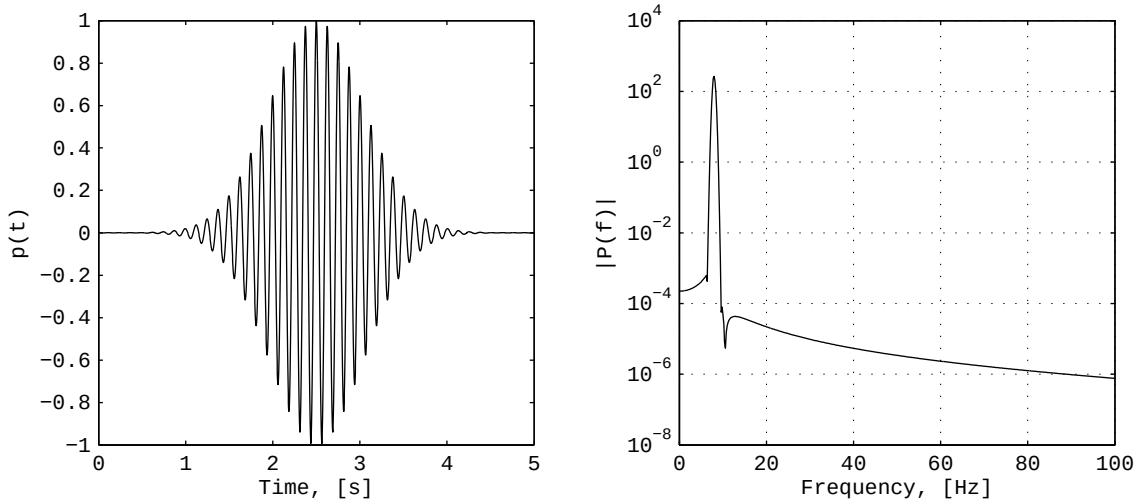

Abbildung 1.5: Morlet wavelet impulse (time and frequency domain)

In time domain, the Morlet wavelet is a cosine function shaped with a Gaussian bell curve for compact support in time. In frequency domain, the Morlet wavelet shows a narrow peak corresponding to the core frequency Ω of the cosine function. As a result of the uncertainty principle, the width of the peak in frequency domain is related inversely proportional to the width of the pulse in time domain. That is to say, the shorter the pulse the wider the peak.

1.2.3 Mexican Hat wavelet impulse

The definition of the Mexican Hat wavelet, as for the Morlet wavelet, has been taken from [9]:

$$p(t) = \frac{2}{\sqrt{3}}\,\pi^{-\frac{1}{4}}\,\left(1-t^2\right)\,\exp\left(-\frac{t^2}{2}\right) \tag{1.10}$$

The same cosiderations as in the case of the Morlet wavelet equally apply to the Mexican Hat wavelet. Therefore, the corresponding adaptions have been made besides of the transition from complex to real values (because the Mexican Hat wavelet was already defined as a real function). Eq. 1.11 gives the final equation used to define the Mexican Hat wavelet impulse.

$$p(t) = p_0\,\left(1-\frac{(t-\tau)^2}{\sigma}\right)\,\exp\left(-\frac{(t-\tau)^2}{2\,\sigma}\right) \tag{1.11}$$

with

$$\sigma = \left(\frac{w_{eff}}{8.87}\right)^2 \tag{1.12a}$$

w_{eff} = effective width of the pulse, as defined by

$$p\left(\tau \pm \frac{w_{eff}}{2}\right) = 0.001\, p_0 \tag{1.12b}$$

The factor 8.87 in the first part of eq. 1.12 which relates σ to the effective width of the pulse has been determined using the Matlab function fzero for scalar nonlinear zero finding. This was necessary because for the Mexican Hat impulse the second equation in eq. 1.12 is a transcendental function the zeros of which cannot be determined analytically.

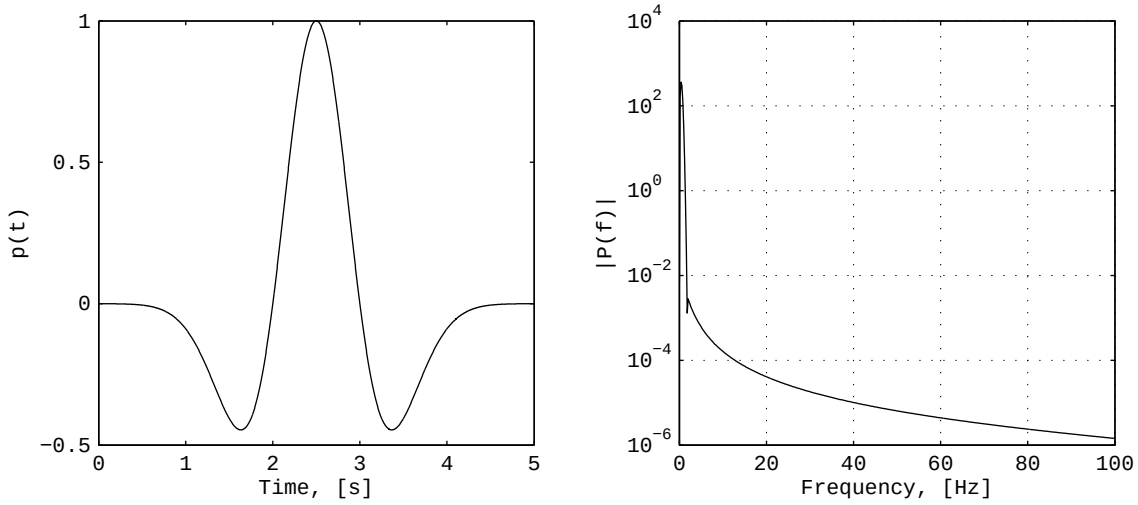

Abbildung 1.6: Mexican hat wavelet impulse (time and frequency domain)

For the Mexcian Hat wavelet, no core frequency can be specified. Thus, the only possibility to excite higher frequency modes is to make the pulse shorter in time in order to broaden the covered frequency range. As the covered frequency range always begins at zero and cannot be shifted, when higher frequency modes are to be excited, a very broad frequency band will be covered. This implies some problems regarding the energy introduced into a specific mode of oscillation.

1.2.4 Shannon wavelet impulse

The original formulation of the Shannon wavelet function in the real domain has been taken from [2]:

$$p_k^n(t) = 2^{n/2}\, \frac{\sin \pi(2^n t - k - 1/2) - \sin 2\pi(2^n t - k - 1/2)}{\pi(2^n t - k - 1/2)} \tag{1.13}$$

The aforementioned adaptions have been applied. In this case, besides the decoupling of pulse width and amplitude, also a transition from a discrete wavelet family to a continuously defined one has been made. The pulse width could not be introduced by simply dividing each t by a corresponding σ as before, because that would have impacted the core frequency as well as the amplitude of the impulse. Therefore, it has been decided to shape the pulse with an

additional gaussian bell curve. Thus, the width of the pulse can be determined independently without significantly changing the frequency content of the original signal. Finally, the following expression has been obtained:

$$p(t) = p_0 \exp\left(-\frac{(t-\tau)^2}{2\,\sigma}\right) \frac{\sin(\Omega\,(t-\tau)) - \sin(2\,\Omega\,(t-\tau))}{\Omega\,(t-\tau)}\,, \qquad p(t=\tau) = -p_0 \tag{1.14}$$

with

$$\sigma = -\frac{w_{eff}^2}{8\,\ln 0.001} \tag{1.15a}$$

w_{eff} = effective width of the pulse, as defined by

$$p\left(\tau \pm \frac{w_{eff}}{2}\right) = 0.001\,p_0 \tag{1.15b}$$

Because for $t = \tau$ the denominator of the last fraction in eq. 1.14 becomes zero, the corresponding value has to be determined analytically by applying l'Hôpital's rule which yields the indicated value. The Shannon wavelet as defined by eq. 1.14 is depicted in fig. 1.7.

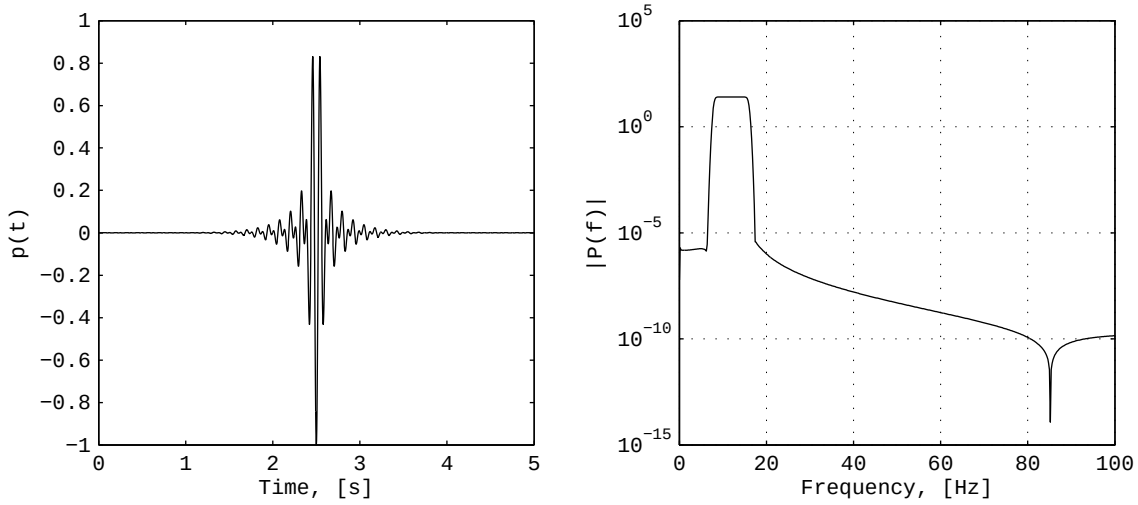

Abbildung 1.7: Shannon wavelet impulse (time and frequency domain)

It is an interesting property of the Shannon wavelet that the plateau to be observed in the frequency domain representation in fig. 1.7 always extends from Ω to $2\,\Omega$ with equal amplitude (corresponding to the angular frequencies of the two sinudoids in eq. 1.14). Thus it is possible to customize the Shannon wavelet to excite a certain frequency band of interest with equal energy over the specified range.

Yet this formulation of the Shannon wavelet comes with an undesirable characteristic: as the width of the plateau is always Ω, an increase of the fundamental frequency corresponds to an

increase in the width of the plateau. Thus, when exciting higher frequency modes, the plateau gets very broad and the energy is introduced over a large frequency band with equal amplitude. This effect is depicted in the diagram on the left hand side of fig. 1.8

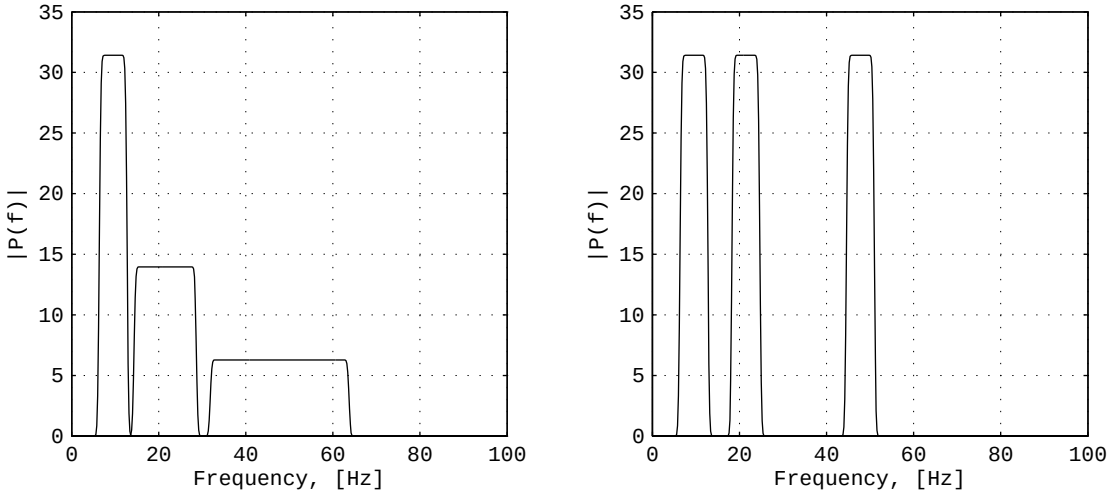

Abbildung 1.8: Comparison of original (left) and modified Shannon wavelet (right)

This effect is undesirable in two respects: on the one hand, the broader plateau does not allow the selective excitation of narrow frequency bands and thus, for instance, the separation of neighbouring structural modes. On the other hand, the comparably low level of the plateau may not provide enough energy input around resonances to sufficiently excite the natural modes of a large and heavy structure like an airplane section. In order to correct this drawback, the original equation has been modified again by introducing two independent angular frequencies, Ω_1 and Ω_2, as well as a normalization factor, a, to make sure that the peak value of the signal remains unchanged. The final equation of the Shannon wavelet as used for further analyses is:

$$p(t) = \frac{p_0}{a} \exp\left(-\frac{(t-\tau)^2}{2\,\sigma}\right) \frac{\sin(\Omega_1\,(t-\tau)) - \sin(\Omega_2\,(t-\tau))}{\Omega_1\,(t-\tau)}\,, \qquad p(t=\tau) = -p_0 \tag{1.16}$$

with

$$a = abs\left(1 - \frac{\Omega_2}{\Omega_1}\right) \tag{1.17}$$

For the definition of σ and the effective width of the pulse refer to eq. 1.14.

1.3 Stochastic excitation

According to [10] there are basically two types of stochastic excitation: white noise and broad-band noise. White noise is characterized by having a constant power density over the whole

spectrum and zero correlation between succesive values, i.e. the autocorrelation function of a white noise signal is a Dirac impulse. As it is impossible for a signal of finite duration to have a constant power density over all frequencies, white noise is a purely theoretical notion which in practice is approximated by broadband noise. Broadband noise is characterized by having a nearly constant power density not over the whole spectrum but over a certain frequency range. The stochastic excitation signals have been implemented in Matlab by generating a series of random numbers and filtering the resulting signal by a bandpass elliptic filter as provided by Matlab via the function ellip.

There exist two different types of broadband noise which are known as gaussian broadband noise and uniformly distributed broadband noise according to the distribution of the random numbers used to generate the signal.

Gaussian broadband noise is based on normally distributed random numbers generated via the Matlab function randn. Its time and frequency domain representation is shown in fig. 1.9:

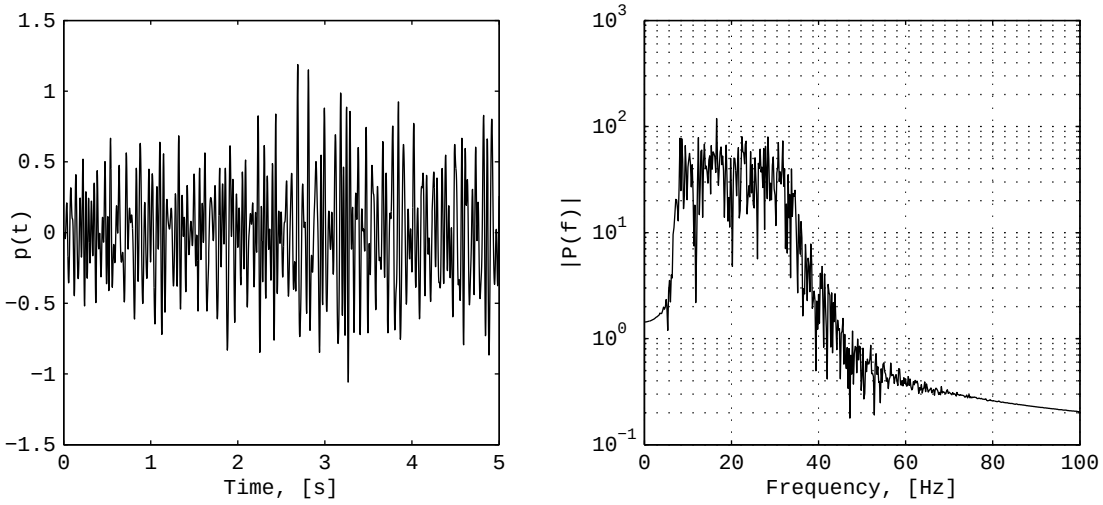

Abbildung 1.9: Gaussian broadband noise (time and frequency domain)

Uniformly distributed broadband noise is based on uniformly distributed random numbers generated via the Matlab function rand. It is depicted in fig. 1.10 in both time and frequency domain:

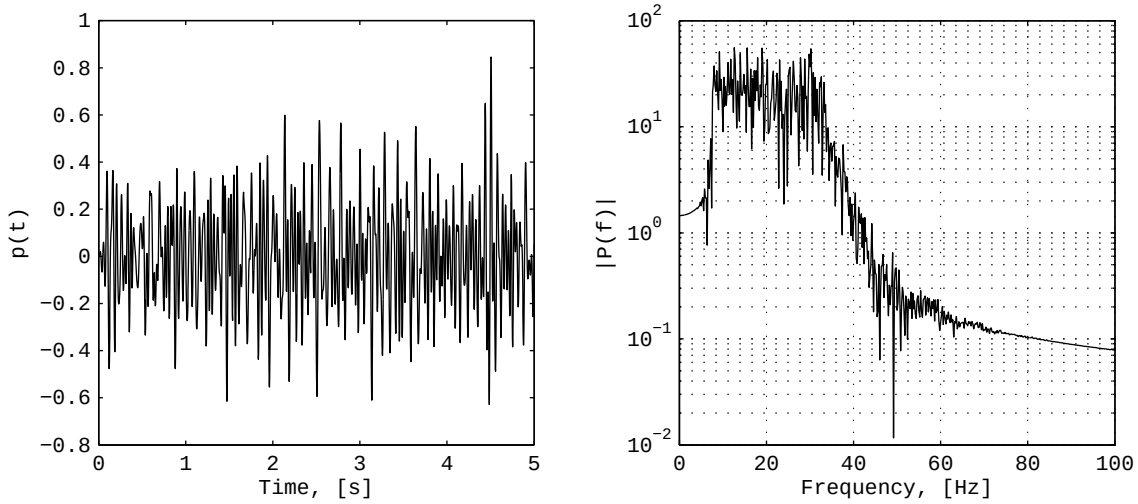

Abbildung 1.10: Uniformly distributed broadband noise (time and frequency domain)

2 Analysis methods

2.1 Introduction

The initial step in experimental modal analysis is to obtain the response of a structure to a certain kind of excitation. This might be accomplished under operational conditions or from modal testing within a controlled test environment. Once the response measurement has been completed, the next step to be performed is the identification of the modal parameters of the structure from the measured data. For this task a broad range of modal analysis techniques have been developed over the past decades. The decision which technique to apply in a given situation is to be based on diverse considerations, the most important of which are: Is the excitation known (which is generally the case in experimental modal analysis) or unknown (which is generally the case in operational modal analysis where the response of the structure to an ambient excitation under operational conditons is measured)? Is the data available just in the frequency domain or also in the time domain? Does a reasonable estimation of the parameters exist as a starting point for an iterative procedure to improve the initial guess? Are the structural modes well seperated or closely spaced? Is it reasonable to assume a lightly damped structure?

There are several critera for the classification of modal analysis techniques. He and Fu distinguish between single-degree-of-freedom (SDoF) and multi-degree-of-freedom (MDoF) methods [6]. Natke classifies modal analysis techniques as either phase resonance methods (Phasenresonanzverfahren) or phase separation methods (Phasentrennungstechnik, [10]). Phase resonance methods are based on an adaption of the excitation in such a way that only one single mode is excited which simplifies the post-processing of the thus obtained data quite a lot but is experimentally very extensive. Phase separation methods on the other hand shift most of the effort to the post-processing of the data as quite elaborate and computationally expensive numerical methods are required to extract reliable modal information from data comprising the coexistent contribution of several modes. The most widely-used classification however distinguishes between frequency domain methods and time domain methods. This classification shall also be adopted in the present work. The following list gives an overview of some popular modal analysis techniques as presented in [6], [10] and [5]:

I - Frequency domain methods

- Peak-picking method
- Circle-fit method
- Inverse FRF method

- Least-squares method
- Dobson's method
- Rational Fraction Polynomials
- Lightly Damped Structures

II - Time domain methods

- Least-squares time domain method
- Ibrahim time domain (ITD) method
- Random Decrement (RD) method
- ARMA Time Series method
- Least-squares Complex Exponential (LSCE) method

The methods chosen to be examined in the present work are the Circle-fit method as a frequency domain method as well as the Least-squares Complex Exponential (LSCE) method and the Random Decrement method as time domain methods. In the following section the basic mathematics and definitions needed for a thorough understanding of those advanced methods shall be described, followed by a detailed presentation of the aforementioned modal analysis techniques.

2.2 Basics

In this section the mathematical basics for the understanding of the examined modal analysis techniques shall be derived and the fundamental terms and definitions shall be introduced. First, the basic concept of the Fourier Transform (FT) is explained followed by the transition from the Continuous FT (CFT) to the Discrete FT (DFT) which is essential for the practical implementation of the method as computers are only able to deal with discrete data. Subsequently, a few remarks on the effect of leakage and the concept of windowing to reduce this effect are to complete this presentation. At the end of the section the very important concept of the Frequency Response Function (FRF) which is the basis for all the frequency domain methods of modal analysis is introduced and the most important characteristics of an FRF are discussed.

2.2.1 Fourier Transform

The Fourier Transformation or Fourier Transform is a very fundamental mathematical instrument of signal analysis. Originally developed by Fourier for the solution of differential equations in the area of heat conduction, it soon was applied to totally different problems throughout the various disciplines of science and engineering. Initially developed as an analytical instrument and therefore constrained to the application to analytically defined and integrable functions, the real power of the Fourier Transform could only be exploited with the advent of modern computers.

In the following section the process of adapting the original version of the FT, the CFT, via the Fourier Series (already discretized in frequency but not yet in time) to a fully discretized version processable by computers, the DFT, is outlined, and the most important characterictics of the FT with respect to its application in signal analysis are discussed. The formulation of the FT as presented here is taken from [1]. For a mathematically complete and rigorous derivation would be beyond the scope of the present work, only the most important steps and results are covered here and the interested reader is recommended to consult [1] for further details.

Continuous Fourier Transform

The CFT of a continuous function of time, $p(t)$, is defined by:

$$P(f) = \int_{-\infty}^{+\infty} p(t)\, e^{-j2\pi ft}\, dt \tag{2.1}$$

Normally, $p(t)$ is considered a function of time and $P(f)$ is considered a function of frequency, with lower case letters denoting the time function and upper case letters denoting its corresponding Fourier Transform. The CFT can be interpreted as developing a function (which not necessarily needs to be periodic) into an infinite series of sinusoids and cosinusoids where the trigonometric functions form an orthogonal basis of the function space which $p(t)$ is part of. For convenience a complex presentation of the CFT is normally preferred and this complex notation is also adopted throughout the present work. The inverse FT is defined by:

$$p(t) = \int_{-\infty}^{+\infty} P(f)\, e^{j2\pi ft}\, df \tag{2.2}$$

The relationship between a function of time, $p(t)$, and its frequency domain equivalent, $P(f)$, is commonly denoted by the following symbolism:

$$p(t) \;\circ\!\!-\!\!\bullet\; P(f) \tag{2.3}$$

There exist several slightly different definitions of the CFT, with a common alternative definition given by:

$$P(j\,\omega) = a_1 \int_{-\infty}^{+\infty} p(t)\, e^{-j\,\omega\,t}\, dt\,, \qquad \omega = 2\,\pi\,f \tag{2.4a}$$

$$p(t) = a_2 \int_{-\infty}^{+\infty} P(j\,\omega)\, e^{j\,\omega\,t}\, d\omega \tag{2.4b}$$

with the condition

$$a_1\, a_2 = \frac{1}{2\,\pi} \tag{2.4c}$$

As the CFT is based on continous functions and infinite integrals whereas a computer can only deal with discrete values and finite sums, the continuous version of the FT is not suited for processing with modern digital computers. Therefore, an alternative formulation of the Fourier Transform discretized in both time and frequency had to be developed with the Fourier Series constituting a first step in the course of this development.

Fourier series

It can be shown that a periodic function $p(t)$ with period T_0 can be developed into an infinite Fourier Series of the form

$$p(t) = \sum_{n=-\infty}^{+\infty} \alpha_n\, e^{\,j2\pi n f_0 t} \tag{2.5a}$$

with the coefficients defined by

$$\alpha_n = \frac{1}{T_0} \int_{-T_0/2}^{+T_0/2} p(t)\, e^{-j2\pi n f_0 t}\, dt\,, \qquad n = 0,\, \pm 1,\, \pm 2,\, \ldots \tag{2.5b}$$

Here, $f_0 = 1/T_0$ denotes the fundamental frequency of $p(t)$. This constitutes a first step towards a fully descretized FT as here the frequency already is a discrete quantity while time is still continuous. This series expansion is also necessary for the mathematically rigorous transition from the continuous to the discrete version of the FT as the DFT implicitly assumes the discrete time series of finite duration it is applied to to be but one period of a periodic signal of infinite duration.

Discrete Fourier Transform

For the derivation of the Discrete Fourier Transform from the Continuous Fourier Transform basically three steps have to be performed:

I - Sampling of the continuous signal $p(t)$ with the sampling interval T to obtain a discretized version of the signal consisting of the sample values $p(k\,T),\ k = -\infty,\, \ldots\,,\, -1,\, 0,\, 1,\, \ldots\,,\, \infty$

II - Time limitation of the infinite time series $p(k\,T)$ by multiplication with the rectangular function

$$x(t) = \begin{cases} 1, & -\frac{T}{2} < t < T_0 - \frac{T}{2} \\ 0, & \text{otherwise} \end{cases}$$

where T_0 is the duration of the limiting function (observation period).

III - Sampling of the CFT of the finite time series $p(k\,T)$, $P(f)$, with a sampling rate of $\Delta f = 1/T_0$ in the frequency domain to complete the modification of the original continuous FT pair to the desired discrete FT pair.

After completing all these steps the following representation of the DFT is derived:

$$p(kT) = \frac{1}{N} \sum_{n=0}^{N-1} P\left(\frac{n}{N\,T}\right) e^{\,j2\pi nk/N} \;\circ\!\!-\!\!\bullet\; P\left(\frac{n}{N\,T}\right) = \sum_{k=0}^{N-1} p(kT)\, e^{-j2\pi nk/N} \tag{2.6}$$

As for the CFT, several slightly different definitions of the DFT exist. The one given by eq. 2.6 is the one adopted by Matlab [8].

Eq. 2.6 shows that the unit of the DFT coefficients is the same as that of the original time series. However, the size of the DFT coefficients is still dependent on the numer of sampling values N. Thus, for the DFT coefficients to truly represent the same physical quantity as the original time series, the DFT as computed by Matlab's `fft` function has to be normalized by multiplication with the factor $1/N$. Furthermore, a multiplication with the factor 2 is needed to correct the effect of aliasing. If the original time series is a structural displacement response consisting of a superposition of several different vibration modes, the thus normalized DFT will give the actual physical amplitudes of the respective oscillations. Remebering the formula for the vibration energy of an SDoF system of stiffness k oscillating with an amplitide of $\hat{x}$, $W = 1/2\,k\,\hat{x}^2$, the square of the modulus of the normalized DFT gives a measure of the vibration energy of a system at any given frequency.

It is important to keep in mind that the sampling process in both time and frequency domain implies a periodicity of the discrete frequency and time domain series as expressed by the following equations:

$$P\left(\frac{n}{N\,T}\right) = P\left[\frac{(r\,N+n)}{N\,T}\right], \qquad r = 0,\, \pm1,\, \pm2,\, \ldots \tag{2.7a}$$

$$p\,(k\,T) = p\,[(r\,N+k)\,T], \qquad r = 0,\, \pm1,\, \pm2,\, \ldots \tag{2.7b}$$

The consequences of this implied periodicity will be discussed in the next section.

The practical implementation of the DFT is commonly realized by means of the Fast Fourier Transform (FFT) algorithm. Several versions of the FFT exist, the most popular being the version presented by Cooley and Tukey in the 1960s [4]. The FFT algorithm allows a much more effective computation of the DFT in comparison to the direct computation. This is essential for

the processing of practical measurement data which often comprises a huge number of sampling values.

2.2.2 Leakage and windowing

As previously mentioned (cf. eq. 2.7), the DFT implies a periodicity of the underlying sampled signal. If the sampling time constitutes an integer multiple of the fundamental period of the sampled signal, the periodic continuation of the signal is smooth and the DFT accords with the CFT of the corresponding continuous signal (cf. fig. 2.2-a). If, however, the sampling time is not equal to an integer multiple of that fundamental period, a sharp discontinuity is induced which leads to non-zero side lobes in the DFT that are purely numerical and do not correspond to any frequency component effectively present in the sampled signal. This effect is known as leakage and as it considerably distorts the DFT of the signal (cf. fig. 2.2-b) it is desirable to weaken that effect. This can be achieved by multiplying the sampled signal with a so-called window function which weakens the discontinuity and therefore reduces the effect of leakage. There are many different window functions, each with their characteristic advantages and drawbacks. One of the most common window functions is the Hamming window which is implemented in Matlab according to eq. 2.8 and is graphically depicted in fig. 2.1. This window has been employed throughout the present work for the purpose of leakage reduction and its effect can be seen in fig. 2.2-c.

$$w(n) = 0.54 - 0.46 \cos\left(2\pi \frac{n}{N}\right) , \qquad 0 \leq n \leq N \tag{2.8}$$

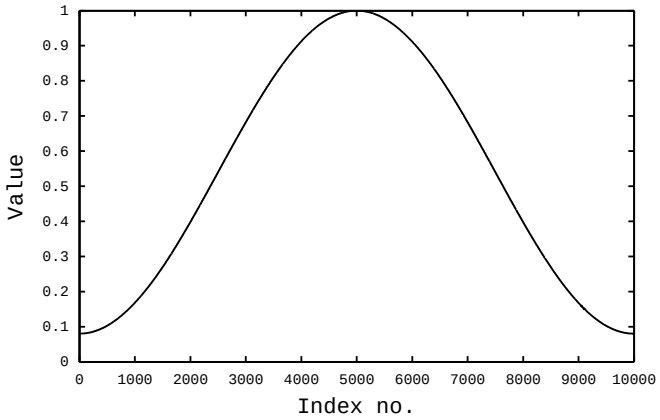

Abbildung 2.1: Hamming window function as implemented in Matlab

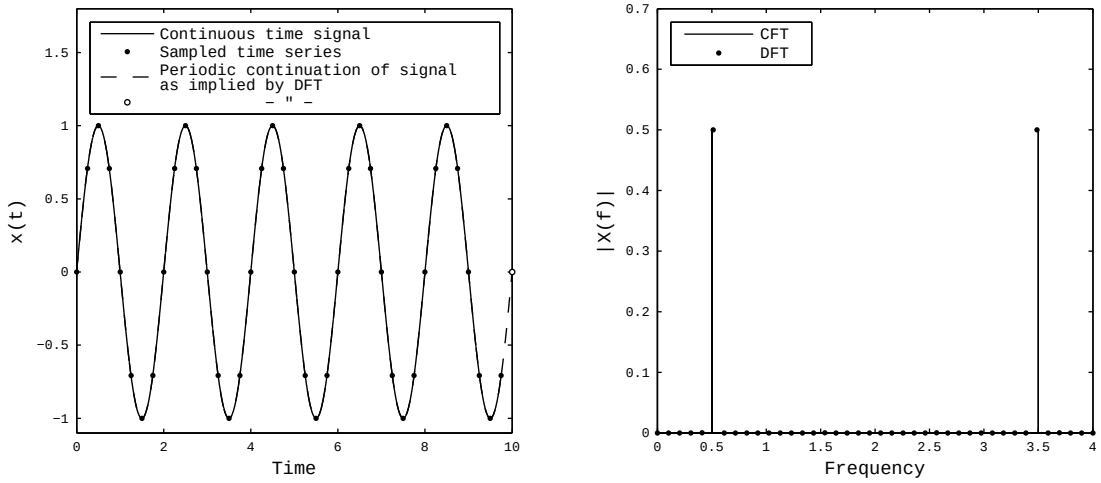

(a) Sampling time is integer multiple of fundamental period → smooth continuation

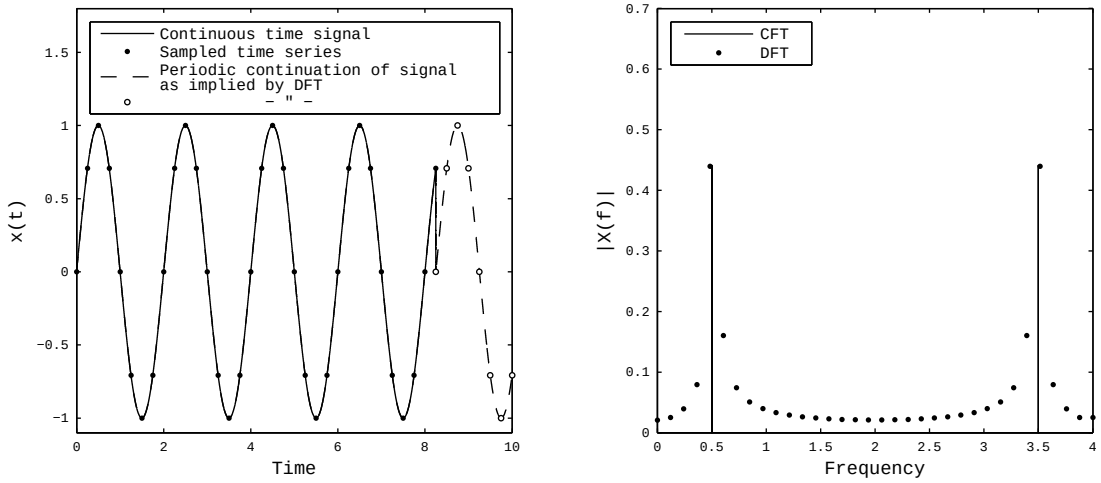

(b) Sampling time is no integer multiple of fundamental period → strong discontinuity induced

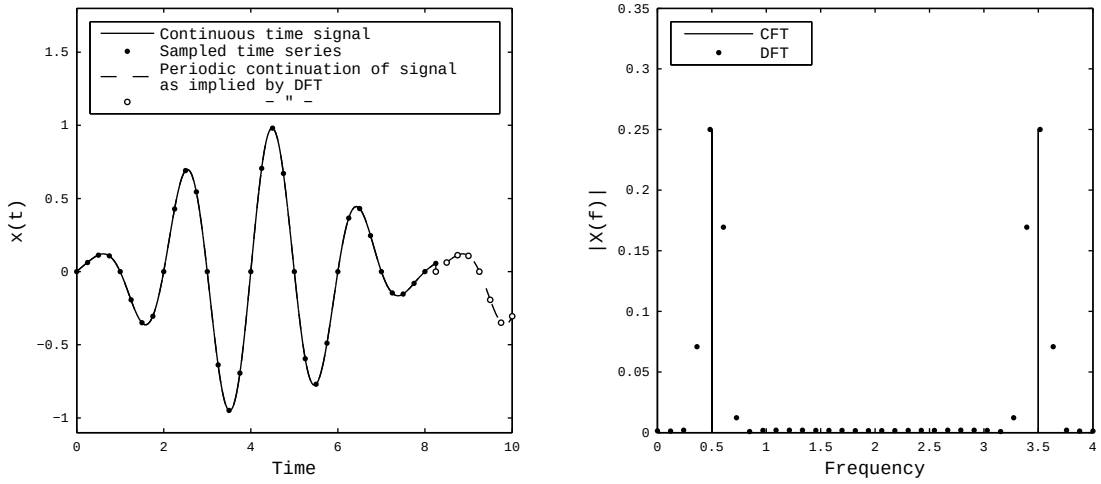

(c) Sampling time is no integer multiple of fundamental period, data windowed with Hamming window → discontinuity weakened

Abbildung 2.2: Leakage and windowing

2.2.3 Frequency Response Function (FRF)

SDoF systems

A very basic concept for all modal analysis techniques based on frequency domain data ist the Frequency Response Function (FRF) of a system. The mathematical derivation presented in this section as well as the nomenclature used throughout the present work is based on the formulation given in [5].

Starting with the general equation of motion of a viscously damped SDoF system

$$m\,\ddot{x} + c\,\dot{x} + k\,x = f(t) \tag{2.9}$$

a solution to the special case where $f(t) = 0$ (free vibration) can be obtained by using the generic trial solution

$$x(t) = x\,e^{s\,t} \tag{2.10}$$

where s is a complex quantity. Inserting this approach in eq. 2.9 yields the condition

$$m\,s^2 + c\,s + k = 0 \tag{2.11}$$

which leads to the following values of s for which the differential equation is satisfied:

$$\begin{aligned} s_{1,2} &= -\frac{c}{2\,m} \pm \frac{\sqrt{c^2 - 4\,k\,m}}{2\,m} \\ &= -\omega_r\,\zeta \pm j\,\omega_r\,\sqrt{1-\zeta^2} \end{aligned} \tag{2.12}$$

where $\omega_r = \sqrt{k/m}$ is the resonance angular frequency of the system and $\zeta = c/c_0 = c/(2\,\sqrt{k\,m})$ is the dimensionless damping factor. This result implies a modal solution of the form:

$$x(t) = x\,e^{-\omega_r\zeta t}\,e^{j\,(\,\omega_r\sqrt{1-\zeta^2}\,)\,t} = x\,e^{-at}\,e^{j\omega_r' t} \tag{2.13}$$

This formula describes a harmonic vibration with the damped eigenfrequency $\omega_r' = \omega_r\,\sqrt{1-\zeta^2}$ the amplitude of which is exponentially decaying over time with the decay rate $a = \zeta\,\omega_r$. If we now give up the assumption of a freely vibrating system by introducing an external force, $f(t) = F(j\,\omega)\,e^{j\omega t}$, the forced response of a SDoF system can be deduced. A trial solution of the form $x(t) = X(j\,\omega)\,e^{j\omega t}$ (with ω being the forcing frequency), when inserted into the general

equation of motion 2.9, yields the following solution for the amplitude $X(j\,\omega)$ (in frequency domain, i.e. as a function of frequency):

$$X(j\,\omega) = \frac{F(j\,\omega)}{(k - \omega^2\,m) + j\,(\omega\,c)} \tag{2.14}$$

Physically interpreted, this means that the system responds to the external force $f(t)$ with a harmonic vibration with the forcing frequency ω and an amplitude and phase shift as determined by the complex quantity $X(j\,\omega)$. With the general definition of the FRF,

$$\text{FRF} := \frac{\mathit{Response}}{\mathit{Excitation}} = \frac{X(j\,\omega)}{F(j\,\omega)}\,, \tag{2.15}$$

i.e. the ratio of a system's response to the corresponding excitation computed in frequency domain, we get the following expression for the FRF of the considered SDoF system:

$$\alpha(j\,\omega) = \frac{1}{(k - \omega^2\,m) + j\,(\omega\,c)} \tag{2.16}$$

This special case of an FRF where the regarded response parameter is the displacement $x(t)$ is called Receptance FRF. It is possible to define alternative Frequency Response Functions by selecting either velocity or acceleration instead of displacement as the response parameter. With the relationships $v(t) = \dot{x}(t) = j\,\omega\,x\,e^{j\,\omega\,t}$ resp. $a(t) = \ddot{x}(t) = -\omega^2\,x\,e^{j\,\omega\,t}$ we get the following expressions:

$$\text{Mobility FRF} \;:\; Y(j\,\omega) := \frac{\dot{X}(j\,\omega)}{F(j\,\omega)} = j\,\omega\,\alpha(j\,\omega) \tag{2.17a}$$

$$\text{Accelerance FRF} \;:\; A(j\,\omega) := \frac{\ddot{X}(j\,\omega)}{F(j\,\omega)} = -\omega^2\,\alpha(j\,\omega) \tag{2.17b}$$

It is also possible to define more quantities by using the reciprocal values of the aforementioned definitions. An overview of the various FRF quantities is given in tab. 2.1.

Tabelle 2.1: Overview of FRF quantities (cf. [5])

Response Parameter R	Standard R/F	Inverse F/R
Displacement	Receptance Admittance Dynamic Compliance Dynamic Flexibility	Dynamic Stiffness
Velocity	Mobility	Mechanical Impedance
Acceleration	Inertance Accelerance	Apparent Mass

MDoF systems

As in practical applications one never gets to deal with SDoF systems it is essential for the practical applicability of the concept to generalize the considerations about the FRF as discussed before to MDoF systems. Beginning with the general equation of motion a damped MDoF system with viscous damping,

$$\Big[M\Big]\,\Big\{\ddot{x}\Big\} + \Big[C\Big]\,\Big\{\dot{x}\Big\} + \Big[K\Big]\,\Big\{x\Big\} = \Big\{f\Big\}\ , \tag{2.18}$$

when assuming a harmonic excitation of the form $f(t) = F(j\,\omega)\,e^{j\,\omega\,t}$ the general form of the Receptance FRF of a viscously damped MDoF system shows to be the following:

$$\Big[\alpha(j\,\omega)\Big] = \Big[K + j\,\omega\,C - \omega^2\,M\Big]^{-1} \tag{2.19}$$

When assuming a diagonal damping matrix with an individual damping factor ζ_r for each mode (modal damping), the individual modes of the system become decoupled from one another. Thus, by transforming this expression to modal space, an alternative presentation of the Receptance FRF of an MDoF system which proves to be very useful in practice can be derived:

$$\alpha_{j\,k}(j\,\omega) = \sum_{r=1}^{N} \frac{({}_r\Phi_j)\,({}_r\Phi_k)}{(k_r - \omega^2\,m_r) + j\,(\omega\,c_r)} \tag{2.20a}$$

with

$$c_r = 2\,\zeta_r\,\sqrt{k_r\,m_r} \tag{2.20b}$$

where ${}_r\Phi_j$ denotes the j^{th} component of the r^{th} eigenvector of the system. The corresponding

result for the Mobility FRF is:

$$Y_{j\,k}(j\,\omega) = j\,\omega\,\alpha_{j\,k}(j\,\omega) = \sum_{r=1}^{N} \frac{j\omega \cdot ({}_r\Phi_j)\,({}_r\Phi_k)}{(k_r - \omega^2\,m_r) + j\,(\omega\,c_r)} \tag{2.21}$$

This equation shows that the FRF of a proportionally damped MDoF system can be seen as the linear combination of the contributions of all the individual modes with these contributions being of the same form as an SDoF system's FRF (cf. eq. 2.16 and 2.17). This is a result that will prove to be of great importance in connection with the so-called Circle-fit method which will be derived in the following section.

When dealing with the FE model of a structure, there are two possibilities to determine the FRF of the system: one can directly compute the FRF in frequency domain using the formulas given by eq. 2.19 or eq. 2.20. Alternatively, a transient simulation can be conducted and the FRF at a given point can be computed as the ratio of the structural reponse at that point to the excitation in frequency domain. Obviously, when dealing with a real structure in experimental modal testing, the latter is the only possibility to determine the FRF. Theoretically, when the excitation is applied as a force and the structural oscillation is given enough time to stabilize, both approaches should yield the same result and it should be possible to compute the correct FRF from transient measurement data.

2.3 Frequency domain analysis

There are various methods for the determination of the modal parameters of a system from experimental data. Some of them are based on the measured time response of the system (which is usually the acceleration response) while others operate in the frequency domain.

In this section, one of the most widely used frequency domain modal analysis methods, the Circle-fit method, shall be mathematically derived and discussed in detail. The presentation of the method as given here is based upon that outlined in [5].

2.3.1 Circle-fit method

If one takes a closer look at the Mobility FRF of a viscously damped SDoF system,

$$Y(j\,\omega) = j\,\omega\alpha(j\,\omega) = \frac{j\,\omega}{k - \omega^2\,m + j\,\omega\,c} = \frac{\omega^2\,c + j\,\omega\,(k - \omega^2\,m)}{(k - \omega^2\,m)^2 + (\omega\,c)^2} \tag{2.22a}$$

with

$$Re(Y) = \frac{\omega^2\,c}{(k - \omega^2\,m)^2 + (\omega\,c)^2} \tag{2.22b}$$

and

$$Im(Y) = \frac{\omega\,(k - \omega^2\,m)}{(k - \omega^2\,m)^2 + (\omega\,c)^2} \tag{2.22c}$$

one notes that for

$$U = \left(Re(Y) - \frac{1}{2\,c} \right) \quad \text{and} \quad V = Im(Y)$$

the following relationship holds:

$$U^2 + V^2 = \frac{\left((k - \omega^2\,m)^2 + (\omega\,c)^2 \right)^2}{4\,c^2\,\left((k - \omega^2\,m)^2 + (\omega\,c)^2 \right)^2} = \left(\frac{1}{2\,c} \right)^2 \tag{2.23}$$

The geometrical interpretation of this formula is that a plot of $Im(Y)$ vs. $Re(Y)$ for $\omega = 0 \rightarrow \infty$ will trace out a circle of radius $1/(2\,c)$ with its centre located at $(\, Re(Y) = 1/(2\,c)\,,\; Im(Y) = 0\,)$. The plot on the right-hand side of fig. 2.3 clearly illustrates this property of the Mobility FRF of a viscously damped SDoF system.

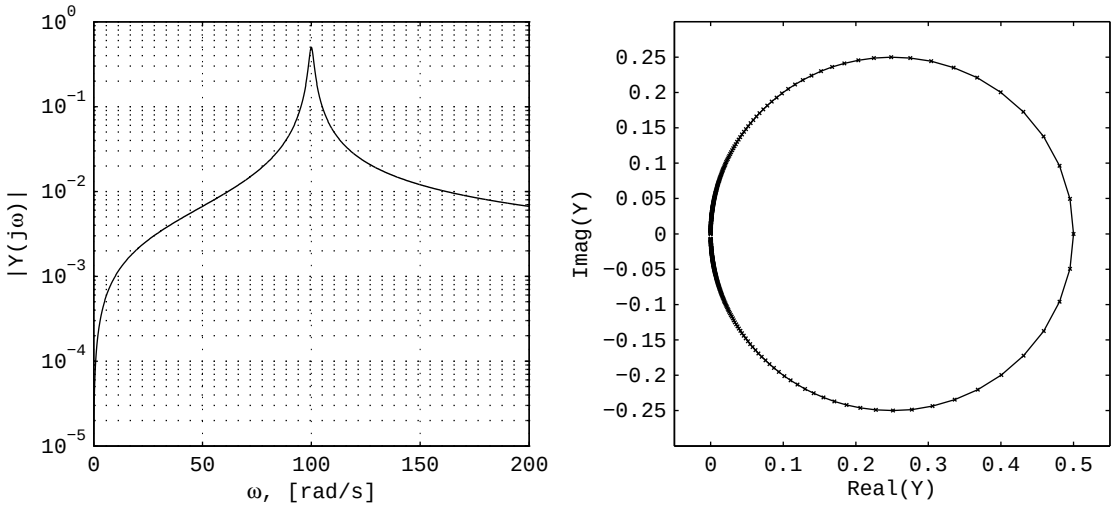

Abbildung 2.3: Mobility FRF of viscously damped SDoF system - Amplitude (left) and Nyquist plot (right)

Dealing with an MDoF system, eq. 2.21 can be rewritten in the following form:

$$Y_{j\,k}(j\,\omega) = \frac{j\,\omega \cdot {}_rA_{j\,k}}{\omega_r^2 - \omega^2 + j2\zeta_r\omega_r\omega} + \sum_{\substack{s=1,\\ \neq r}}^{N} \frac{j\,\omega \cdot {}_sA_{j\,k}}{\omega_s^2 - \omega^2 + j2\zeta_s\omega_s\omega} \tag{2.24a}$$

with

$${}_rA_{j\,k} = ({}_r\Phi_j)\,({}_r\Phi_k) \quad , \quad {}_sA_{j\,k} = ({}_s\Phi_j)\,({}_s\Phi_k) \tag{2.24b}$$

Now, the so-called SDoF assumption is that if one considers only a frequency range in the close vicinity of a resonance frequency of an MDoF system, the FRF will be so strongly dominated by the term corresponding to the mode under examination that the collective contribution of all the other modes remains nearly constant throughout the considered frequency range. Mathematically, this assumption can be expressed as follows:

$$Y_{j\,k}(j\,\omega)|_{\,\omega\sim\omega_r} \simeq \frac{j\,\omega\cdot {}_rA_{j\,k}}{\omega_r^2-\omega^2+j2\zeta_r\omega_r\omega} + {}_rB_{j\,k} \tag{2.25}$$

In practice, this assumption is often found to hold pretty well, especially for well separated modes. Fig. 2.4 illustrates this point for the Mobility FRF of a 3 DoF system with eigenfrequencies at $\omega_1 = 50$ rad/s, $\omega_2 = 100$ rad/s and $\omega_3 = 150$ rad/s.

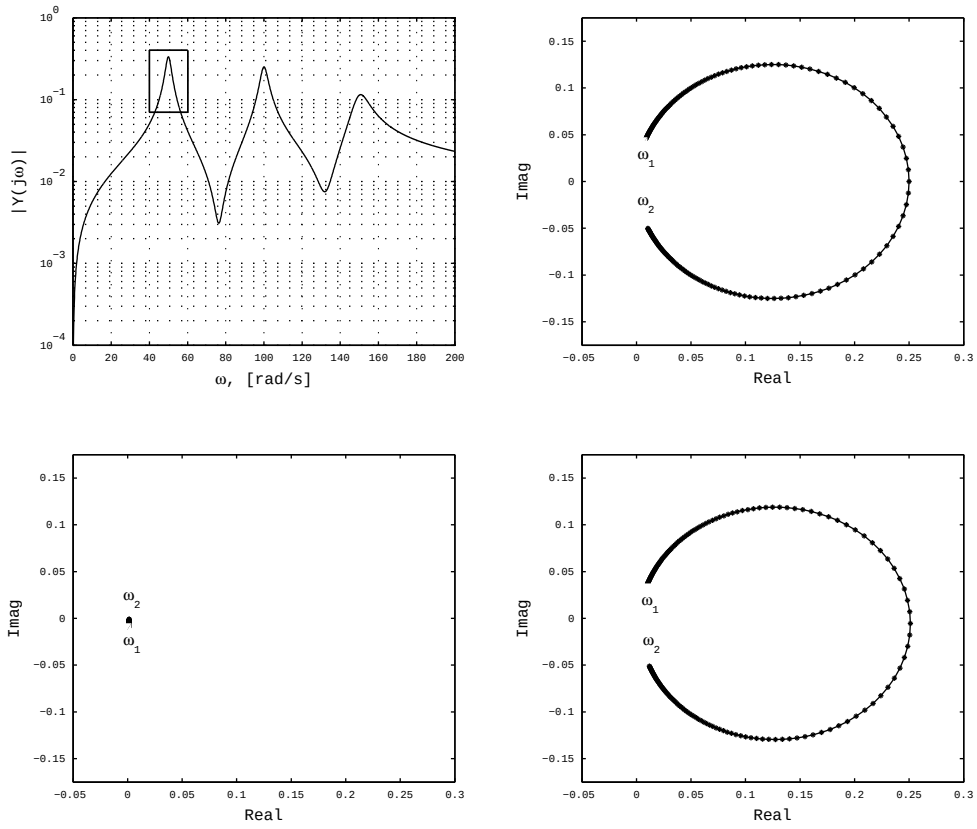

Abbildung 2.4: Illustration of SDoF assumption. From top left to bottom right: Amplitude plot of 3 DoF system, Nyquist plot of first term, second term and total referring to eq. 2.25 (in vicinity of mode 1)

As fig. 2.4 shows, if one deals with the Mobility FRF of a viscously damped system near a resonance it will be very well approximated by eq. 2.25. Recalling eq. 2.23, one notes that eq. 2.25 describes a circle in the complex plane which is just displaced by adding the complex constant ${}_rB_{j\,k}$ as well as scaled and rotated by multiplication with the complex constant ${}_rA_{j\,k}$. It will be shown that the functionality of the Circle-fit method is based upon the distribution of

the complex FRF values along the modal circle. As this basic property of the modal circle is not changed by the operations of scaling, rotating and displacing the circle in the complex plane, we might just as well deal with the easier SDoF expression:

$$Y(j\,\omega) = \frac{j\,\omega}{k - \omega^2\,m + j\,\omega\,c} \tag{2.26}$$

with

$$Re(Y) = \left(\omega^2\,c\right) \;/\; \left((k - \omega^2\,m)^2 + (\omega\,c)^2\right)$$

$$Im(Y) = \left(\omega\,(k - \omega^2\,m)\right) \;/\; \left((k - \omega^2\,m)^2 + (\omega\,c)^2\right)$$

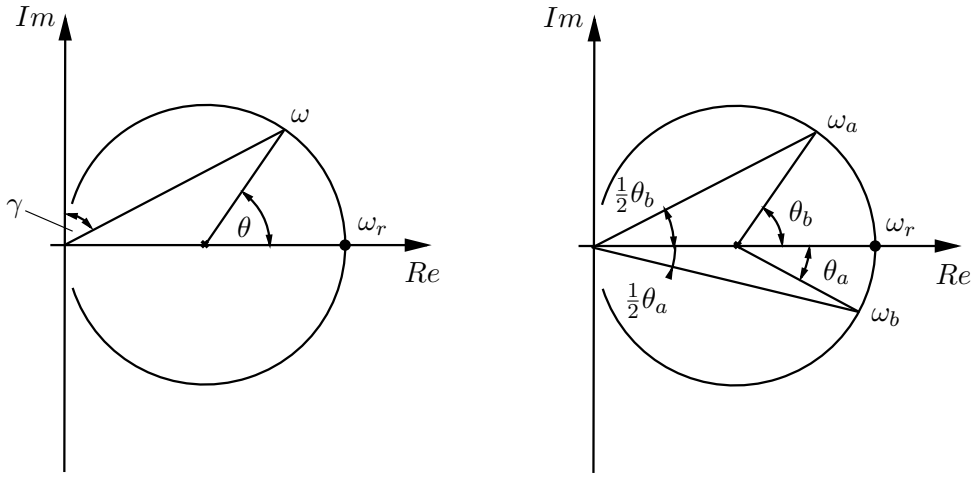

Abbildung 2.5: Geometric properties of modal circle

In combination with the geometric relations to be seen in fig. 2.5, one gets to the following expression:

$$\tan\left(\,\theta/2\,\right) = \omega\left(\,k - \omega^2\,m\,\right) / \left(\,\omega^2\,c\,\right) = \left(\,1 - (\omega/\omega_r)^2\,\right) / \left(\,2\,\zeta\,\omega/\omega_r\,\right) \tag{2.27}$$

If now one considers two points a and b with $\omega_a > \omega_r$ and $\omega_b < \omega_r$ the following equations are derived:

$$\tan\left(\,\theta_b/2\,\right) = \left(\,1 - (\omega_b/\omega_r)^2\,\right) / \left(\,2\,\zeta\,\omega_b/\omega_r\,\right) \tag{2.28a}$$

$$\tan\left(\,\theta_a/2\,\right) = \left(\,(\omega_a/\omega_r)^2 - 1\,\right) / \left(\,2\,\zeta\,\omega_a/\omega_r\,\right) \tag{2.28b}$$

Combining these, one finally arrives at an expression for the damping factor ζ:

$$\zeta = (\omega_a^2 - \omega_b^2) / \{ 2\,\omega_r (\omega_a \tan (\theta_a/2) + \omega_b \tan (\theta_b/2)) \} \tag{2.29}$$

To be able to apply the above described procedure for the determination of the damping factor ζ, the resonance frequency ω_r of the mode under examination is needed. For structural damping, the following (exact) criterion for the determination of ω_r can be analytically derived from the expression for the Receptance FRF:

$$d/d\omega \, (d\omega^2/d\theta) = 0 \quad \text{for} \quad \omega = \omega_r \, , \tag{2.30}$$

which means that the rate of change of ω^2 when plotted versus θ reaches its minimum value at the resonance frequency ω_r. In practice, the derivations in eq. 2.30 were computed using finite differences. Then, the zero-crossing point was determined using linear interpolation. As mentioned above, while this criterion is exact when dealing with structurally damped systems, for viscously damped systems it merely presents an estimation. Therefore, an iterative procedure has been established to improve the initial guess as obtained by application of that criterion. Because an abort criterion is needed for the iteration, a quantitative measure of the quality of an estimation of ω_r had to be established. A closer look at eq. 2.29 shows that by this formula it is possible to compute an estimation of ζ for any possible combination of ω_a and ω_b. For the correct resonance frequency all those estimates should theoretically be the same, even though in practice they will slightly fluctuate around the correct value due to noise and numerical inaccuracies. If the estimate of ω_r is imprecise, however, the obtained values for ζ will show a considerable bias. This fact is illustrated in fig. 2.6. For the creation of the plot as well as for the assessment of the algorithm, an artificial Mobility FRF has been created using the analytical formula given in eq. 2.25. As testing system a 3 DoF system with the following modal parameters has been chosen:

Tabelle 2.2: Modal parameters of the testing system

mode no.	f_r, [Hz]	ω_r, [rad/s]	damping factor ζ, [-]
1	7.96	50	0.03
2	15.92	100	0.02
3	23.87	150	0.01

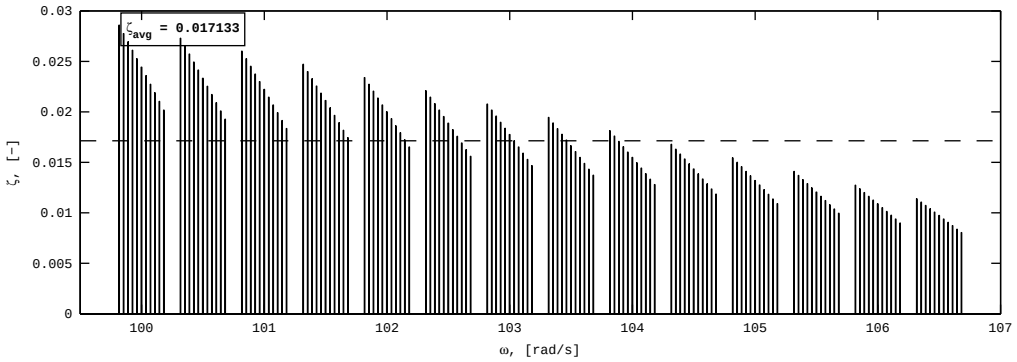

(a) Bad estimate of ω_r

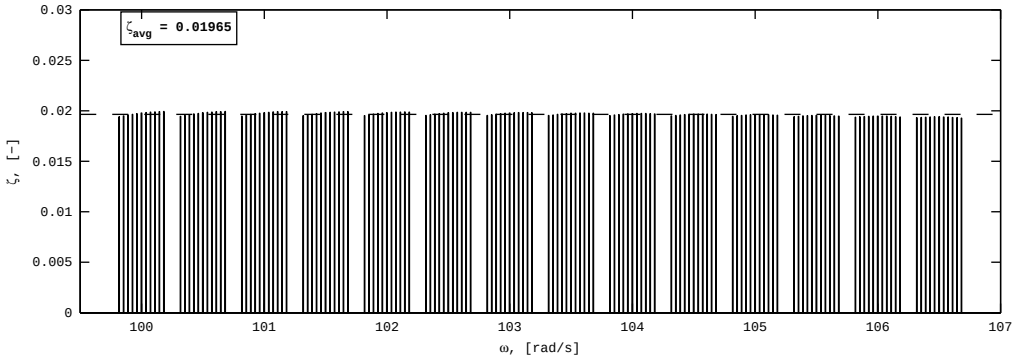

(b) Good estimate of ω_r

Abbildung 2.6: Estimates of damping factor ζ obtained with different combinations of ω_a and ω_b

Based on this characteristic, a minimization of the standard deviation of the various damping estimates,

$$\sigma = \sqrt{\frac{1}{N}\sum_{i=1}^{N}(\zeta_i - \bar{\zeta})^2} \tag{2.31a}$$

with

$$\bar{\zeta} = \frac{1}{N}\sum_{i=1}^{N}\zeta_i \tag{2.31b}$$

has been chosen as a quantitative measure of the quality of an estimate of ω_r. Starting from the initial frequency estimate based on eq. 2.30, a step in both directions is taken and the corresponding standard deviation of the damping estimates is computed. The direction corresponding to a decline in standard deviation, i.e. a smoothing of the damping estimates, indicates the location of the exact resonance frequency. Subsequently, the resonance frequency estimate is iteratively improved by taking a number of steps in that direction until a predefined tolerance limit for the standard deviation is reached.

Fig. 2.7 shows the result delivered by the Circle-fit method when applied to the second mode of

the testing system. The results for all three modes are given by tab. 2.3. A comparison with the values of tab. 2.2 shows that the results are very accurate. Thus precision and reliability of the algorithm have been confirmed.

Tabelle 2.3: Results of Circle-fit method when applied to testing system

mode no.	ω_r, [rad/s]	damping factor ζ, [-]
1	49.999	0.0296
2	99.994	0.0196
3	149.997	0.0099

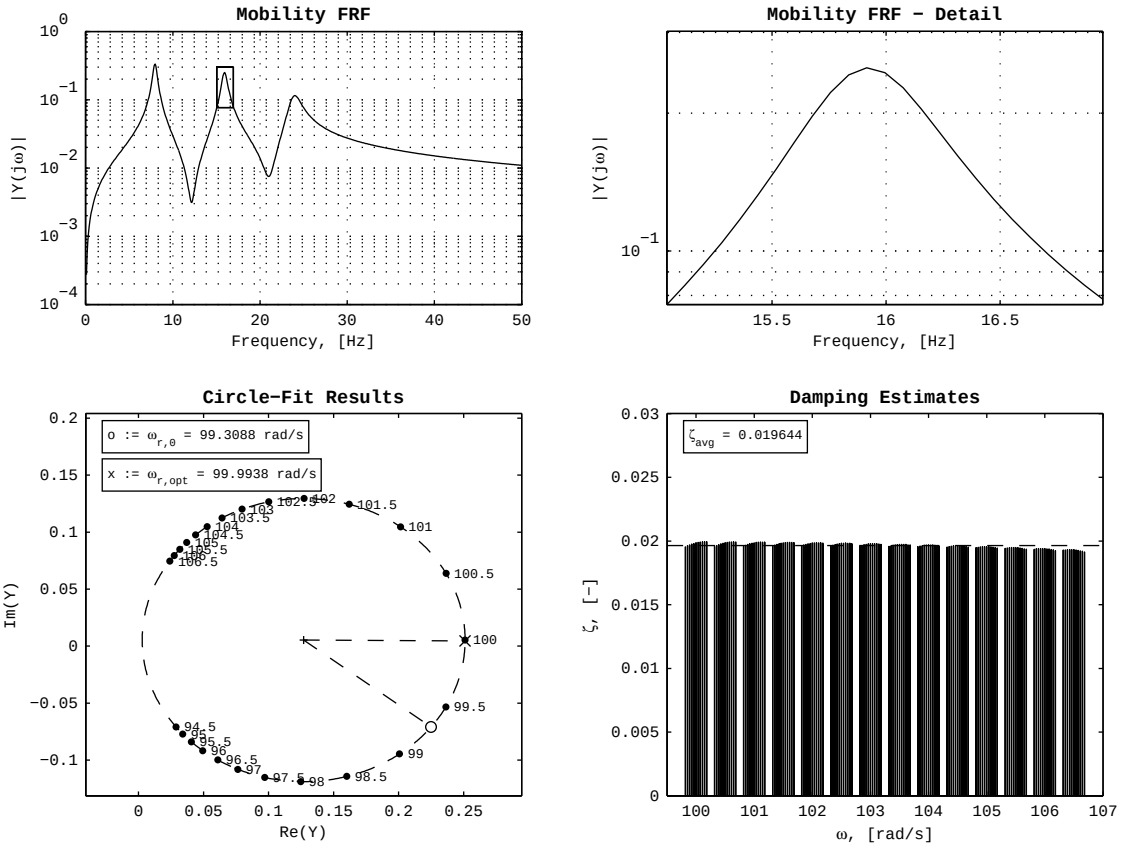

Abbildung 2.7: Results of Circle-fit method for second mode of testing system

For the determination of the circle which fits best the considered data points, the Matlab function CircleFitByTaubin.m by Nikolai Chernov which is available free of charge under [3] is used.

2.4 Time domain analysis

A different approach to determine the modal characteristics of a structure is the analysis based on the measured time response of the structure. This approach presents several advantages

in comparison to frequency domain modal anaylsis. On the one hand, as time domain modal analyis is not based on FRF data, it can be applied even in the case when the excitation is unknown (a characteristic especially valuable in operational modal analysis). Furthermore, in order to obtain accurate FRF data the excitation needs to be applied for a certain time span so that the structural vibration reaches a stabilized state. With time domain analyis, however, accurate modal parameters can be determined in combination with short excitation pulses. The main drawback to time domain modal analysis methods is that they are more sensitive to the presence of noise in comparison to frequency domain methods, therefore requiring a high signal-to-noise ratio to yield reliable results.

2.4.1 Least-squares Complex Exponential (LSCE) method

The first time domain method to be discussed is the Least-squares Complex Exponential (LSCE) method, also known as Prony's method. The mathematical derivation of the method as presented here is taken from [6].

The basis of the LSCE method is the formulation of the free vibration (impulse response) of a structure as a sum of complex exponentials, i.e. damped sinusoids.

$$h_{ij}(t) = \sum_{r=1}^{2N} {}_rA_{ij}\, e^{s_r t} \tag{2.32}$$

Here, the subscript r denotes the contribution of the r^{th} structural mode and the subscript ij denotes the reaction of the structure at DoF i when excited at DoF j, a notation taken from the concept of the Frequency Response Function (cf. section 2.2.3).

Omitting the subscript ij for simplicity and assuming the free vibration data to be present at a series of equally spaced time intervals $k\Delta$ ($k = 0, 1, \ldots, 2N$), one arrives at the following expression:

$$h\,(k\Delta) = \sum_{r=1}^{2N} {}_rA_{ij}\, e^{s_r k\Delta} \quad (\,k = 0,\, 1,\, \ldots\,,\, 2N\,) \tag{2.33a}$$

or

$$h_k = \sum_{r=1}^{2N} {}_rA_{ij}\, z_r^k \quad (\,k = 0,\, 1,\, \ldots\,,\, 2N\,)\ ,\ \ z_r^k = e^{s_r k\Delta} \tag{2.33b}$$

As all the data samples are real-valued, the quantities ${}_rA_{ij}$ and s_r respectively z_r have to be either real-valued or in the form of complex conjugate pairs so that the imaginary parts cancel out each other and thus sum up to a real value.

As any polynomial of degree $2N$ with only real coefficients has $2N$ roots in the form of either real values or complex conjugate pairs, the z_r of the above equation can be interpreted as the

roots of a polynomial:

$$\beta_0 + \beta_1 z_r + \beta_2 z_r^2 + \ldots + \beta_{2N-1} z_r^{2N-1} + \beta_{2N} z_r^{2N} = 0 \tag{2.34}$$

If one now multiplies each of the $2N+1$ equalities of eq. 2.33 with the corresponding coefficient β_k and adds all the equalities together, the following equation is obtained:

$$\sum_{k=0}^{2N} \beta_k h_k = \sum_{k=0}^{2N} \beta_k \sum_{r=1}^{2N} {}_r A_{ij} z_r^k \tag{2.35}$$

or

$$\sum_{k=0}^{2N} \beta_k h_k = \sum_{r=1}^{2N} {}_r A_{ij} \sum_{k=0}^{2N} \beta_k z_r^k \tag{2.36}$$

The sum at the right-hand side of eq. 2.36 is equal to the polynomial defined by eq. 2.34. Thus, a simple linear relationship between the coefficients of the polynomial and the sampled time data can be established:

$$\sum_{k=0}^{2N} \beta_k h_k = 0 \tag{2.37}$$

Without loss of generality, β_{2N} can be assigned to be one, leading to the expression of a given sample value as a linear combination of the $2N$ preceding values, with the β_k being the coefficients of the so obtained auto-regressive scheme. The $2N$ equations needed to determine the $2N$ coefficients can be obtained by formulating the auto-regressive scheme for $2N$ consecutive values, thus arriving at the following system of linear simultaneous equations:

$$\begin{bmatrix} h_0 & h_1 & h_2 & \cdots & h_{2N-1} \\ h_1 & h_2 & h_3 & \cdots & h_{2N} \\ \vdots & \vdots & \vdots & \vdots & \vdots \\ h_{2N-1} & h_{2N} & h_{2N+1} & \cdots & h_{4N-2} \end{bmatrix} \begin{Bmatrix} \beta_0 \\ \beta_1 \\ \vdots \\ \beta_{2N-1} \end{Bmatrix} = \begin{Bmatrix} h_{2N} \\ h_{2N+1} \\ \vdots \\ h_{4N-1} \end{Bmatrix} \tag{2.38}$$

If more than $2N$ equations are taken into account, the least-squares solution is obtained.

With the known coefficents β_k, the roots z_r of the polynomial 2.34 can be easily computed. These roots are related to the complex natural frequencies of the system as given by eq. 2.33. The complex natural frequencies can be expressed in terms of undamped natural frequencies ω_r and damping factors ζ_r as follows:

$$s_r = -\zeta_r \omega_r + j \sqrt{1 - \zeta_r^2}\, \omega_r \tag{2.39a}$$

$$s_r^* = -\zeta_r\,\omega_r - j\,\sqrt{1-\zeta_r^2}\,\omega_r \tag{2.39b}$$

That given, the natural frequency and damping ratio of the r^{th} mode can be directly computed from the corresponding polynomial root by the following relationships:

$$\omega_r = \frac{1}{\Delta}\,\sqrt{\ln z_r\ \ln z_r^*} \tag{2.40a}$$

and

$$\zeta_r = -\frac{\ln(\,z_r\,z_r^*\,)}{2\,\omega_r\,\Delta} \tag{2.40b}$$

Finally, the amplitudes of the computed modes are obtained by solving the following system of equations:

$$\begin{bmatrix} 1 & 1 & \cdots & 1 \\ z_1 & z_2 & \cdots & z_{2N} \\ \vdots & \vdots & \vdots & \vdots \\ z_1^{2N-1} & z_2^{2N-1} & \cdots & z_{2N}^{2N-1} \end{bmatrix} \begin{Bmatrix} {}_1A_{ij} \\ {}_2A_{ij} \\ \vdots \\ {}_{2N}A_{ij} \end{Bmatrix} = \begin{Bmatrix} h_0 \\ h_1 \\ \vdots \\ h_{2N-1} \end{Bmatrix} \tag{2.41}$$

The LSCE method as implemented in the present work uses $2N$ equations and therefore $4N$ data points for the auto-regressive scheme of eq. 2.38. As the dynamic simulations have been conducted with a time step of Δt = 5E-04 s, the usage of directly succeeding data points has proven not to be practical because the time range covered by these data points is too short for a reasonable number of modes. Rather, the data points are selected by the algorithm so that they are evenly spread over the time range to be analysed. As indicated in [5], the results given by the LSCE method depend heavily on the number of modes used. To find the optimum number of modes, an optimization loop has been implemented computing the results for $N = 1 \ldots 50$ and determining the optimum by minimizing the sum of square errors of the reconstructed time domain data. The algorithm has shown to deliver the most reliable and precise results when applied to a time range comprising about 40 to 50 cycles of the main vibration component to be analysed.

The results delivered by the LSCE method when applied to the artificial testing system previously used to verify the functionality of the Circle-fit method (cf. 2.3.1) are shown in fig. 2.8 and tab. 2.4 respectively.

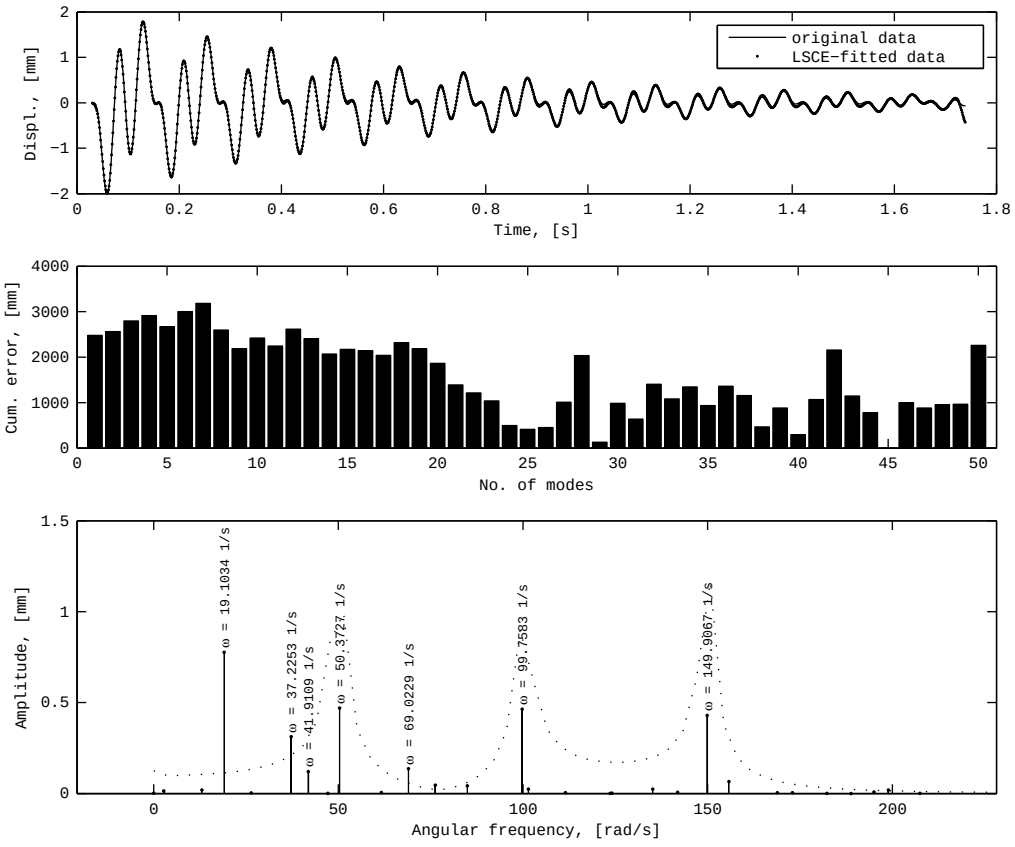

Abbildung 2.8: Results of LSCE method when applied to testing function

Tabelle 2.4: Results of LSCE method when applied to testing function (only results with considerable amplitude listed)

no.	amplitude, [mm]	ω, [rad/s]	damping factor ζ, [-]
1	0.77621	19.103	0.979
2	0.47023	50.373	0.030
3	0.46399	99.758	0.022
4	0.42987	149.907	0.009
5	0.31234	37.225	0.378
6	0.13614	69.023	0.116
7	0.12046	41.911	0.122

Tab. 2.4 shows that the method as implemented delivers precise results even when applied to a superposition of vibrational modes of quite different frequencies. When there is only one dominating frequency component, the above mentioned criterion of selecting a time span comprising 40 to 50 cycles can be applied and the results are even more precise. Furthermore, from tab. 2.4 one can see that there are always a number of so-called computational or numerical modes delivered by the method which account for effects such as noise or inaccurate data. These do

not represent genuine structural vibration modes and can normally be easily identified on the basis of their unusually high damping factors and/or very low amplitudes as indicated in [5]. Further decision support with respect to the distinction of genuine and computational modes can be gained by comparing the LSCE results with the peaks of the DFT (cf. fig. 2.8).

2.4.2 Random Decrement method

Another technique used in time domain modal analysis is the Random Decrement method. This method is used to extract the free decay or impulse response from the response of a structure subjected to random or ambient excitation. The so obtained data have to be further processed using time domain modal analysis methods such as the previously described LSCE method in order to determine the modal parameters of the structure. The description of the Random Decrement technique as presented here is basically taken from [6].

The response of a structure subjected to random excitation can be mathematically described as a superposition of the free response due to the initial conditions and the forced response of the structure. Therefore, the response at time $t_0 + t$ can be decomposed into three parts: the free response of the structure due to the initial displacement X_0 at time t_0, the free response due to the initial velocity $\dot{X}_0$ at time t_0 and the forced response caused by the external forces acting on the structure:

$$x(t+t_0) \;=\; x(t+t_0)\big|_{x(t_0)} \;+\; x(t+t_0)\big|_{\dot{x}(t_0)} \;+\; x(t+t_0)\big|_{f(t)} \tag{2.42}$$

If one now specifies a trigger condition which marks the beginning of a time segment of a definite length within the response history of the structure, a certain number of response segments of equal length is obtained. All these segments share the trigger condition as a common initial condition. The trigger condition may be a certain amplitude value to be crossed, a certain slope or velocity to be reached or a combination of the two. Here, in accordance with the variant discussed in [6], only an amplitude level is specified as trigger condition. The basic argumentation, however, applies equally if another type of condition is chosen. For brevity, a response segment beginning at time t_1 with an initial displacement X_0 shall be denoted as $X_0(t_1 + \tau)$ in the following. As is shown in [7], the individual segments are allowed to overlap without this having a significant influence on the quality of the results.

These segments can be averaged, the outcome being denoted as $\delta_N(\tau)$ if the average of N segments is computed:

$$\delta_N(\tau) = \frac{1}{N} \sum_{r=1}^{N} X_0(t_r + \tau) \tag{2.43}$$

If the excitation is assumed to be zero-mean uncorrelated noise, an assumption often being valid in the case of ambient excitation such as earthquake, wind or wave loading, the average taken

of a sufficiently large number of segments shows an interesting characteristic: as the structural velocities corresponding to the trigger times appear with alternating signs and random absolute values, the part of eq. 2.42 which corresponds to the free response of the structure due to a certain initial velocity will be averaged out. Furthermore, due to the random nature of the excitation and therefore also the response, the forced response part in eq. 2.42 will also be averaged out:

$$\sum_{r=1}^{N} X_0(t_r+\tau)\Big|_{\dot{x}(t_0)} \to 0 \qquad \sum_{r=1}^{N} X_0(t_r+\tau)\Big|_{f(t)} \to 0 \tag{2.44}$$

That is to say, when the average of a sufficiently large number of segments is computed, the remaining part will be the free reponse of the structure due to an initial displacement step input corresponding to the specified trigger value. The so obtained free response, which is commonly referred to as the *randomdec signature* $\delta(\tau)$, can then be analyzed with some other time domain modal analyis method such as the LSCE method in order to determine the modal parameters of the structure.

The basic concept of the Random Decrement method as previously described is illustrated in fig. 2.9.

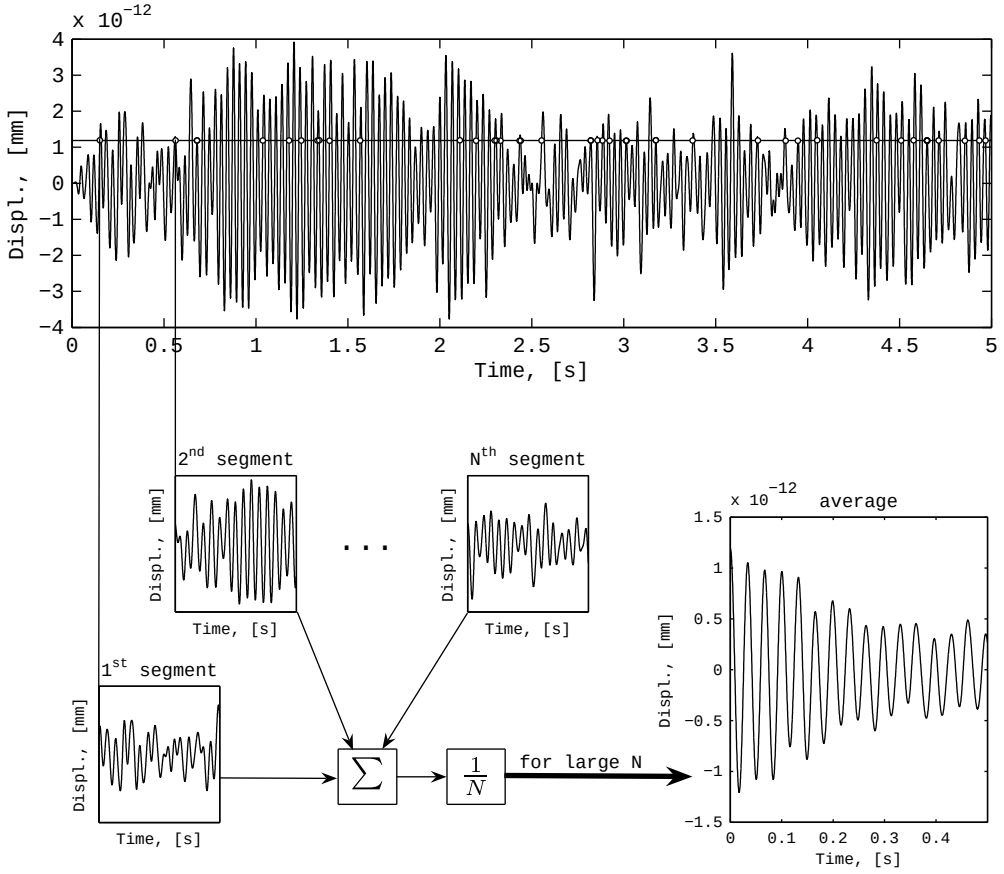

Abbildung 2.9: Schematic depiction of the Random Decrement method

It can be analytically shown that for an MDoF system the free response at any DoF i due to an initial value at a certain DoF j can be obtained when applying the above described procedure to DoF j and simultaneously averaging the corresponding time segments for any other DoF i. For the mathematical derivation of this characteristic of the Random Decrement method the user may refer to [6].

Bibliography

[1] E. O. Brigham, *FFT ; schnelle Fourier-Transformation*, Einführung in die Nachrichtentechnik, München ; Wien : Oldenbourg, 5^{th} ed., 1992.

[2] C. Cattani, *Shannon Wavelets Theory*, Mathematical Problems in Engineering, 2008.

[3] N. Chernov, *Circle Fit (Taubin Method)*, `http://www.mathworks.com/matlabcentral/fileexchange/22678`, January 2009.

[4] J. W. Cooley and J. W. Tukey, *An Algorithm for the Machine Computation of the Complex Fourier Series*, in Mathematics of Computation, vol. 19, April 1965, pp. 297–301.

[5] D. J. Ewins, *Modal Testing: Theory and Practice*, Research Studies Press Ltd., 1984.

[6] J. He and Z.-F. Fu, *Modal Analysis*, Butterworth-Heinemann, 2001.

[7] T. Kijewski and A. Kareem, *Reliability Of Random Decrement Technique For Estimates Of Structural Damping*, in 8th ASCE Specialty Conference on Probabilistic Mechanics and Structural Reliability.

[8] The MathWorks, *MATLAB Version 7.1 Release 14 with Service Pack 3 - Product Documentation, 2005.*

[9] X. Mi, H. Ren, Z. Ouyang, W. Wei, and K. Ma, *The use of the Mexican Hat and the Morlet wavelets for detection of ecological patterns*, in Plant Ecology, vol. 179, Springer, e-mail: kpma@ibcas.ac.cn; phone: +86-10-62836223; fax: +86-10-82599518, 2005, pp. 1–19.

[10] H. G. Natke, *Einführung in Theorie und Praxis der Zeitreihen- und Modalanalyse: Identifikation schwingungsfähiger elastomech. Systeme*, Braunschweig; Wiesbaden: Vieweg, 1983.